

# Experimental Verification of the Sectored Annular Phased Array for MRI Guided Ultrasound Surgery

T. FJELD AND K. HYNYNEN, Department of Radiology, Brigham and Women's Hospital and Harvard Medical School, Boston, MA 02115.

*Abstract* – To meet two of the requirements for MRI Guided Ultrasound Surgery, namely small surgical equipment and large focal volumes, a combined array encompassing the design parameters of the concentric-ring array and the sector-vortex array has been proposed. Simulations will show that the sectored annular array is capable of producing larger necrosed tissue volumes than the concentric-ring alone, while maintaining the ability of the concentric-ring array to move the focal volume in the axial direction of the array. These simulations are verified by measurements of the acoustic fields produced by an experimental array in water. In addition, the constructed array produced the necessary power required to coagulate tissue in rabbit thigh *in vivo*, while the temperature elevation was monitored using MRI.

## I. INTRODUCTION

Conventional MRI magnets have small openings which place space restrictions on ultrasound transducers and the mechanical positioning assembly used for ultrasound surgery. One possible solution to this problem is to use the concentric-ring array design to allow electrical positioning of the focus in the depth direction rather than mechanical positioning [1]. Mechanical motion in the depth direction accounts for the majority of the surgical equipment volume that reduces space available for patient positioning. However, as is the case with single focus transducers, the focal volume produced by the concentric ring is very small (approximately 1-4 mm across the focus). Previous studies have shown that smaller focal volumes require more sonications and a longer treatment time than larger focal volumes [2].

Previous studies have shown that a focused transducer diced into wedge shaped sectors (the sector-vortex array) can create larger focal volumes than those produced by a single focus transducer [3,4]. While a previous study has shown that it is theoretically possible to combine the concentric-ring design with the sector-vortex design allowing for simultaneous focal zone movement and enlargement [5], the goal of the current research is to show that it is possible to construct such an array that manipulates the focal volume as expected and can produce enough power to create lesions *in vivo*.

An experimental array has been constructed to verify the previous simulation results. This transducer consists of 13 rings and 4 sectors (52 channels total). Measurements of the acoustic fields produced by the experimental array will be compared to the simulation results. Finally, lesions produced by the experimental array in rabbit thigh *in vivo* will be presented. Proton density images and temperature mapping

MRI data taken during and after the rabbit thigh sonications will be presented.

## II. MATERIALS AND METHODS

### Array Geometry

The sectored annular array geometry consists of a spherically-curved, circular transducer which has first been cut into concentric rings and then diced into wedge-shaped sectors. A schematic of the constructed sectored annular array is shown in Figure 1. The transducer shown is composed of 13 evenly spaced rings divided into 16 sectors. The coordinates used are consistent with MRI coordinates when the transducer is positioned in the bore of the magnet, with the  $y$ -axis corresponding to the anterior/posterior direction, the  $z$ -axis corresponding to the superior/inferior direction, and the  $x$ -axis corresponding to the lateral direction.

A previous parametric study of the concentric-ring transducer design has shown that rings evenly spaced in the  $XZ$ -projection result in a practical transducer with a maximum focal range [1]. Thus, this method of ring spacing has been used for all of the transducer designs that have been studied.

### Calculation of Element Phasing

The element phasing used to produce the multiple focus field patterns result from phasing in the same manner as the simple concentric-ring array and then adding a phase rotation to each individual ring as one would do for the simple sector-vortex array. Thus, the rings in each sector focus along the central axis at the specified depth, however each element in

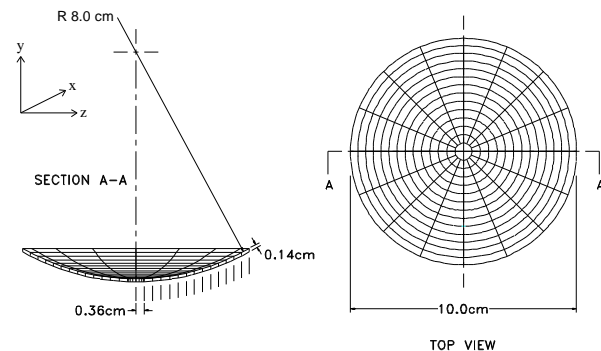


Figure 1. Basic geometry of the constructed sectored annular array. Note that although 16 sectors are shown, the constructed array was comprised of only 4 sectors. The coordinates chosen correspond to MRI coordinates when the transducer is properly mounted in the positioning system.

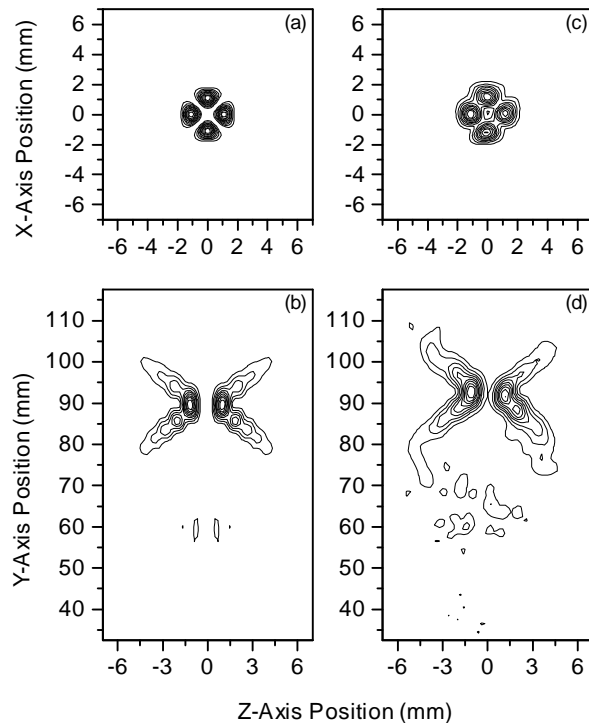


Figure 2. Acoustic field measurements of the sectored annular array operating in mode 2. (a) and (b) correspond to the simulated fields focused at 90 mm. (c) and (d) represent the associated measured fields focused at the same depth.

each sector has a discrete offset from the corresponding elements in the other sectors. In order to both move the focus axially and produce annular foci, both the ring-to-ring phasing in a specific sector and the sector-to-sector phasing on a specific ring must be maintained. For a detailed description of the phase calculations, refer to Fjield and Hynynen, 1996.

#### Field Calculations

Acoustic pressure fields were calculated using a numerical method of summation of simple sources as described by Zemanek [6]. Detailed descriptions of the pressure field calculations can be found in previous works [1,2].

#### Array Construction

The constructed concentric-ring array was machined from a 1.38 mm thick, spherically curved lead zirconate titanate (PZT-4) piezoelectric shell with a diameter of 10 cm. An 8 cm radius of curvature was chosen in order to demonstrate the ability to focus in the near portion of the desired focal range where the transducer's geometric tolerances are most critical. 14 equally spaced rings (in the XZ-plane) were formed by cutting completely through the ceramic between the rings. The space between the rings (about 0.3 mm wide) was filled with silicone rubber. Four sectors were created by removing narrow strips of electrode from the back of the transducer. The ceramic was then mounted in a polycarbonate holder with an air space at the back of the array.

Each element of the array was connected to an LC matching circuit in order to match the array elements to 50  $\Omega$  at the operating frequency of 1.5 MHz. The power and phase of each channel were independently controlled by in-house manufactured amplifier systems. For the beam plots, the RF amplifier system used has 3 bits of amplitude control resolution and 4 bits of phase control resolution [7].

The *in vivo* experiments were conducted using a new amplifier design possessing the ability to produce 0 to 60 watts of RF power per channel. Forward power is self-regulated with internal forward power feedback and is independently controlled from channel to channel. The phases of each channel are independently controlled with 12 bits of resolution. A paper describing the new amplifier technology is forthcoming.

Although 64 channel amplifiers were used, as the innermost ring was neither sectored nor powered, the complete array consisted of 13 rings and 4 sectors, and thus a total of only 52 individual elements were powered.

#### Acoustic Field Measurements

The 13 ring, 4 sector phased-array was placed in a tank of degassed water. Stepper motors scanned a thermistor embedded in a small bead of silicone across the focal region of the transducer [8]. Measurements were taken every 1.0 mm in the axial direction and 0.25 mm in the radial direction. Due to errors resulting from the initial placement of the thermistor in the field, an uncertainty in the absolute location of the field in the axial direction is introduced.

#### In Vivo Experiment

The sectored annular array was placed in a three axis positioning prototype hydraulic positioning device manufactured by General Electric Medical Systems (Milwaukee, WI). The hair from the thighs of a New Zealand white rabbit was removed with clippers and depilatory cream. The rabbit was then anesthetized with a mixture of ketamine and xylazine and placed on its side atop the positioning system. Degassed water was used to provide acoustic coupling between the submerged transducer and the thigh of the rabbit. The rabbit and positioning system was inserted into a standard 1.5 T MRI scanning system (Signa, General Electric Medical Systems, Milwaukee, WI).

Temperature mapping was generated using the temperature-dependent proton resonant frequency shift measured with a fast spoiled gradient echo sequence (FSPGR). The imaging parameters were as follows: repetition time TR = 52.6 ms, echo time TE = 12 ms, flip angle = 30°, bandwidth = 7.2 kHz, resolution 256 x 128, field of view FOV = 16 cm, slice thickness of 3 mm, and an imaging time of 3.5 s. The scanner was programmed to reconstruct the real and imaginary images that were used to calculate the phase difference images. A baseline image taken prior to each sonication was subtracted from the images taken during each sonication to calculate the phase difference induced by tissue heating [9].

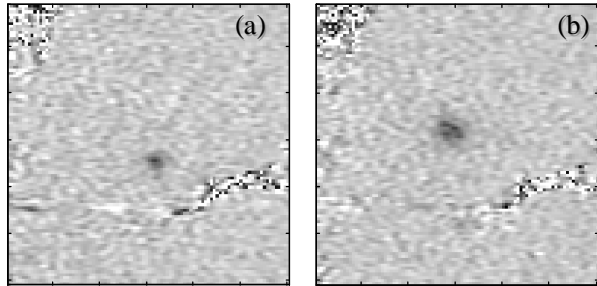


Figure 3. Phase difference image resulting from two 10 s sonications of the sectored annular array. (a) corresponds to mode 0 and (b) corresponds to mode 2. Each image measures 6 cm x 6 cm.

T2-weighted images were taken after the sonications with a fast spin echo (FSE) sequence to evaluate the necrosed tissue volume. The parameters used in these sequences were: repetition time TR = 2000 ms, echo time TE = 68 ms, echo train length = 8, number of data acquisitions = 2 to 3, field of view FOV = 16 cm, and slice thickness = 3 mm.

### III. RESULTS

#### Acoustic Field Measurements

In order to compare the fields produced by the experimental array to the simulated fields, simulations were run using the actual geometry of the constructed array (including dead space between the rings) sonicating into water. Fig. 2(a) compares the theoretical and experimental axial plane pressure-squared intensity distributions at the focal depth of 90 mm using phase rotation mode two for the constructed 13 ring, 4 sector array. The experimental field plot is less sharply focused and shows an error of approximately 2 mm in the axial location of the focus. Fig. 2(b) compares the theoretical and experimental pressure-squared intensity distributions in the focal plane. The experimental fields were similar in shape with the same peak separation and location as the simulated fields. However, the experimental peaks were wider and the field did not reduce to zero between the peaks as is the case with the theoretical results.

#### MRI Monitored In Vivo Experiment

Fig. 3(a) shows the normalized phase difference image in the

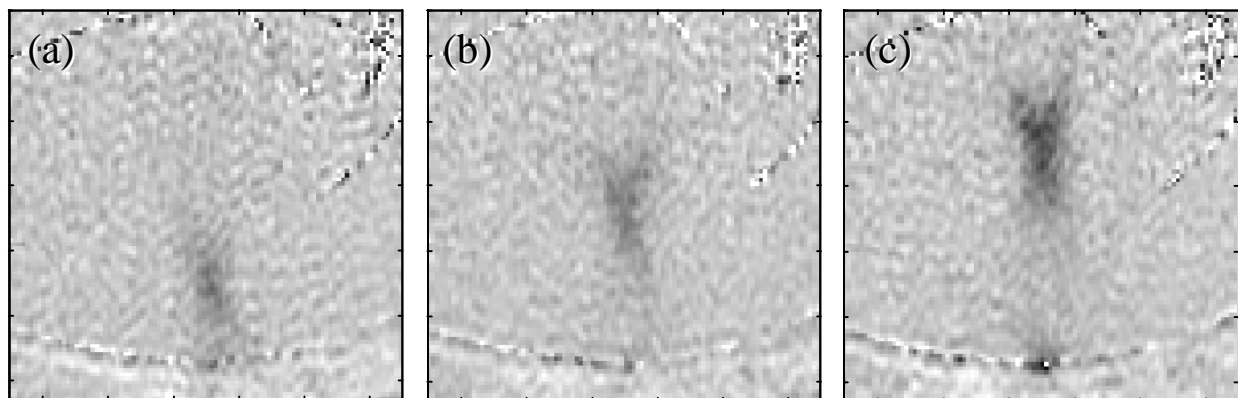


Figure 5. Close-ups of phase difference images showing thermal elevations produced by sectored annular array operating in mode 2. (a) corresponds to a focus at 7 cm, (b) 8 cm, and (c) corresponds to 9 cm. Each image measures 6 cm x 6 cm.

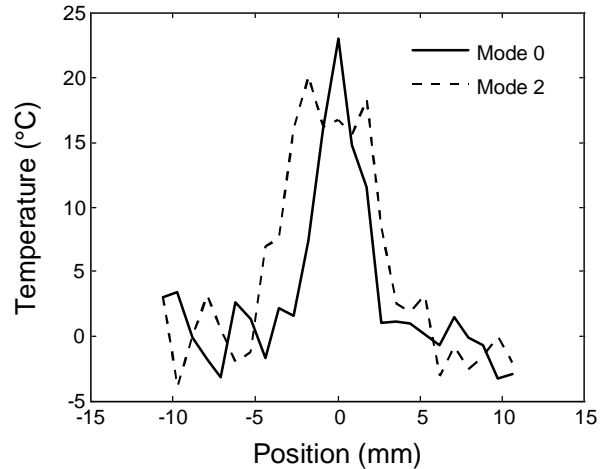


Figure 4. Comparison of peak widths for thermal elevations produced *in vivo* by the sectored annular array operating in mode 0 and mode 2.

focal plane at the end of a 10 s pulse of the array operating in mode 0 at the geometric focus. The total electrical forward power was set to 80 W, however there was 7 W reflected power, resulting in a total transmitted electrical power of 73 W. The maximum temperature elevation induced by the mode 0 sonication was 22.9 °C.

After the tissue temperature returned to the baseline temperature, the transducer was repositioned laterally with the hydraulic positioning system and a second sonication was performed with the array operating in mode 2. The phase difference image in the focal plane for this sonication is shown in Fig. 3(b). For this sonication, the forward power was set to 200 W, which resulted in 182 W total transmitted power. The maximum temperature elevation resulting from this second sonication was 22.3 °C.

Fig. 4 shows the profiles of the temperature elevations induced by the mode 0 and mode 2 sonications. These profiles were obtained from the phase difference images shown in Fig. 3. The full-width half-maximum of the temperature profiles are 3.0 mm and 5.7 mm for mode 0 and mode 2, respectively.

The ability of the sectored annular array to increase and decrease the focal depth while sonicating in mode 2 is

verified in Fig. 5. Three sonications were performed at depths of (a) 70 mm (168 W), (b) 80 mm (167 W), and (c) 90 mm (267 W). The temperature elevations for these three sonications as measured with the phase difference images were (a) 21.0°C, (b) 19°C, and (c) 24°C.

T2-weighted images were taken in the plane across the foci to confirm the creation of lesions. One of these images is shown in Fig. 6. As the image shows, two different sized lesions were formed from the mode 0 and mode 2 sonications.

#### IV. DISCUSSION

The acoustic field plots shown in Figs. 2 demonstrate the ability of the sectored annular array to both move the focus along the central axis and create an annulus of focal zones at that axial depth. The resulting errors in the axial depth of the 90 mm deep focus plots were caused by errors in positioning the hydrophone that was used to set the phases of the experimental transducer.

It is important to note that the older in-house amplifier system with less power control and phase control required manual phasing of the experimental array with a hydrophone. The new amplifier system was constructed primarily in response to the driving requirements of the new array designs composed of elements of varying size and impedance. This new system did not require manual phasing of the experimental array, and the theoretical phases produced the focal patterns that were used to create all of the *in vivo* temperature elevations shown in Figs. 3 and 4.

The power requirements for all of the temperature elevations shown were significantly higher than predicted in the simulations. For example, a mode 2 sonication at the geometric focus should require 55 watts of acoustic power to produce a 63°C temperature elevation. However, the experimental results for the mode 2 sonication shown in Fig. 3 indicate that 205 watts of acoustic power are required,

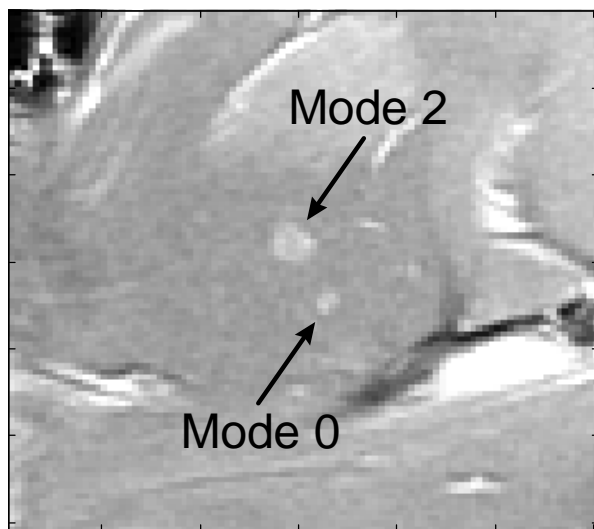


Figure 6. T2-weighted image showing the mode 0 and mode 2 lesions created by the sectored annular array. This image measures 6 cm x 6 cm.

assuming the same 40% transducer efficiency that was measured for a similar concentric-ring array. (Note that the temperature elevations measured axially tend to be lower than measured across the focus due to the difference in voxel geometry.) For mode 0, a similar result is found: the simulated results predict 21 watts while the experimental results indicate an 80 watt requirement. Although the power requirements are higher than expected, each element of a similar array has produced 5 watts acoustic power per square cm. This would result in a total of over 400 acoustic watts, which should result in sufficient power reserve for the therapeutic array.

#### V. CONCLUSION

The present work has shown that it is possible to construct an array that allows the simultaneous movement of the focal region along the central axis of the array and increase the focal volume. The sonications into rabbit thigh *in vivo* have shown that an array constructed in the manner described above is capable of producing enough acoustic power to create lesions in muscle. The next stage in the development of this transducer will be increasing the number of sectors from 4 to 8, as this will result in a transducer with a higher possible mode number and thus a larger focal volume.

#### ACKNOWLEDGMENTS

This work supported by NIH Grant #CA46627-08. Additional support provided by General Electric Medical Systems with the MRI thermal imaging and transducer positioning device.

#### REFERENCES

- [1] T. Fjfield, X. Fan, and K. Hynynen, "A parametric study of the concentric-ring transducer design for MRI guided ultrasound surgery," *J. Acoust. Soc. Am.*, vol. 100, 1996.
- [2] X. Fan and K. Hynynen, "Ultrasound surgery using multiple sonications – treatment time considerations," *Ultrasound Med. Biol.*, vol. 22, pp. 471-482, 1996.
- [3] C. A. Cain and S. Umemura, "Concentric-ring and sector-vortex phased-array applicators for ultrasound hyperthermia," *IEEE Trans. Microwave Theory Tech.*, vol. 34, pp. 542-551, 1986.
- [4] S. Umemura and C. A. Cain, "The sector-vortex phased array: acoustic field synthesis for hyperthermia," *IEEE Trans. Ultrason. Ferroelectr. Freq. Contr.*, vol. 36, pp. 249-257, 1989.
- [5] T. Fjfield and K. Hynynen, "The combined concentric-ring and sector-vortex phased array for MRI Guided Ultrasound Surgery," *submitted to IEEE Trans. Ultrason. Ferroelectr. Freq. Contr. in 1996.*
- [6] J. Zemanek, "Beam behavior within the nearfield of a vibrating piston," *J. Acoust. Soc. Am.*, vol 49, 1971.
- [7] M. T. Buchanan and K. Hynynen, "Design and experimental evaluation of an intracavitary ultrasound phased array system for hyperthermia," *IEEE Trans. Biomed. Eng.*, vol. 41, pp. 1178-1187, 1994.
- [8] C. J. Martin and A. N. R. Law, "Design of thermistor probes for measurement of ultrasound intensity distributions," *Ultrasonics*, pp. 85-90, 1983.
- [9] Y. Ishihara, A. Calderon, H. Watanabe, K. Mori, K. Okamoto, Y. Suzuki, K. Sato, K. Kuroda, N. Nakagawa, and S. Tsutsumi, "A non-invasive temperature mapping using water proton chemical shifts," *Proc., SMRM, 11<sup>th</sup> Annual Scientific Meeting*, Berlin, pp. 4803, 1992.